Tellus (1999), 51A, 195–221
Printed in UK – all rights reserved

TELLUS
ISSN 0280–6495

A reformulation of the background error covariance in the ECMWF global data assimilation system

By J. DERBER[1] and F. BOUTTIER[2]*, [1]NOAA/NCEP, World Weather Building, 5200 Auth Road, Washington DC 20233, USA; [2]ECMWF, Shinfield Park, Reading RG2 9AX, Berks., UK

(Manuscript received 23 July 1998; in final form 23 November 1998)

ABSTRACT

The background error covariance plays an important role in modern data assimilation and analysis systems by determining the distribution of the information in the data in space and between variables. A new formulation has been developed for use in the ECMWF system. The non-separable structure functions depend on the horizontal and vertical scales and a generalized linear balance operator to imply multivariate structure functions. The balance operator is incorporated into the definition of the analysis variables to ensure good preconditioning of the problem. The formulation and structure of the background error covariance are presented, and the implications for the analysis increments are examined. This reformulation became the operational ECMWF formulation in 3D-Var in May 1997 and in 4D-Var in November 1997.

1. Introduction

The spatial and multivariate structure of the analysis increments in 3D-variational (3D-Var) analysis is driven by the formulation of the background error covariance. An optimal design of the background error covariance would ideally reflect the covariances of the short-range forecast errors in the assimilation. In practice, it must be modelled in order to approximate the average variances, autocorrelations and balance properties of the background errors. Between January 1996 and May 1997, the ECMWF 3D-Var operational assimilation system (as well as the experimental 4D-Var) relied on a formulation developed by Heckley et al. (1992) and documented in Courtier et al. (1998), Andersson et al. (1998) and Rabier et al. (1998). In May 1997, a new formulation of the background term was implemented which performs significantly better in both 3D-Var and 4D-Var. The purpose of this paper is to document the revised background error covariance formulation and to explain its advantages in meteorological, technical and scientific terms.

The new background error covariance formulation differs significantly from the previous one, mainly in the tropical structure functions of mass and in the mass/wind coupling of the analysis increments. The specific humidity analysis has not been modified. In the mid-latitudes, the new background error covariance behaves similarly to the previous operational system, except near the surface and near the tropopause where the geostrophic coupling is now weaker and there is some multivariate coupling between the divergence, mass and vorticity fields. The autocovariances are non-separable, with a dependence of the vertical covariances on the horizontal total wavenumber n, as in the previous formulation. However, they are not expressed in terms of the same variables. Therefore, even though the vorticity autocovariances are assumed to be homogeneous and isotropic, the effective vertical correlations of temperature depend on latitude. The multivariate coupling is basically a mass/wind linear balance, as in the previous formulation, but it does not

* Corresponding author.

rely on the Hough normal modes of the model. The new formulation retains all the existing scientific features of the previous formulation with less mass/wind balance in the smaller horizontal and vertical scales and virtually no balance near the equator. There are also some new features including a weak coupling between divergence and vorticity as well as divergence and mass, which may be important in the tropics and near the surface, and a vertical variation in the strength of the balance.

This paper contains a discussion of the new formulation of the background error covariance, first describing the mathematical formulation and calibration of the statistics (Section 2) and then presenting diagnostics of the formulation (Section 3). An evaluation in terms of single observations, assimilation fits to data and forecast statistics is given in Section 4. Conclusions and future work will be discussed in Section 5.

2. Formulation of the background error covariance

The ECMWF analysis and assimilation system performs the update of the forecasts using an incremental procedure. First, the differences between the observations and the background field are estimated using the full resolution of the forecast. The observation increments are then used in the incremental 3D-Var analysis procedure to create a lower resolution analysis increment. The lower resolution analysis increments are used to update the higher resolution background field in order to create the higher resolution analysis. These higher resolution analysis increments are initialized to reduce the effects of the incompatibilities between the resolutions of the forecast model. (See Courtier et al., 1998 for details).

The incremental 3D-Var analysis procedure finds the low-resolution analysis increment x by minimizing the cost function given by:

$$J(x) = J_\mathrm{b}(x) + J_\mathrm{o}(x) + J_\mathrm{c}(x).$$

- The observation term (J_o) measures the fit of the differences between the observation and the high-resolution background to the low-resolution analysis increment.
- The constraint term (J_c) measures the fit of the low-resolution analysis increment to a set of dynamical constraints.

These two terms are not the topic of this paper and are described in more detail in Courtier et al. (1998), Rabier et al. (1998) and Andersson et al. (1998).

- The background term (J_b) measures the fit of the analysis to the background (currently a 6-h forecast).

J_b is given by

$$J_\mathrm{b}(x) = x^\mathrm{T}\boldsymbol{B}^{-1}x \tag{2}$$

where $\boldsymbol{B}$ is the assumed background error covariance matrix. The new formulation of the background error covariance is based on redefining the analysis variables in a way that simplifies the problem but contains the necessary multivariate balances. If a change of variables is defined such that $x = L\chi$ where L is defined such that $L^\mathrm{T}\boldsymbol{B}^{-1}L = I$, then

$$\begin{aligned} J_\mathrm{b}(x) &= \chi^\mathrm{T}\chi, \\ J_\mathrm{c}(x) &= J_\mathrm{o}(L\chi), \\ J_\mathrm{c}(x) &= J_\mathrm{c}(L\chi). \end{aligned} \tag{3}$$

At the initial point of the minimization if $\chi = 0$, then $x = 0$. Note that since it is only necessary to transform χ to x in the minimization procedure (to evaluate J_o and J_c), it is not necessary to define L^{-1} or for L to be invertible.

In this formulation, the background error covariance is not explicitly defined, but implied by the definition of L. The model variables are the vorticity ζ, the divergence η, the temperature and surface pressure (T, p_s), and the specific humidity q. In the new formulation of the background error covariance, the temperature and surface pressure (T, p_s) and divergence η are partitioned into balanced and unbalanced components. Then, L can be further subdivided to be:

$$L = K\boldsymbol{B}_\mathrm{u}^{1/2}, \tag{6}$$

where K is a balance operator transforming the unbalanced variables to the model variables. The $\boldsymbol{B}_\mathrm{u}^{1/2}$ operator is the symmetric square root of the background error covariances $\boldsymbol{B}_\mathrm{u}$ of the unbalanced variables (i.e., $\boldsymbol{B}_\mathrm{u}^{\mathrm{T}/2}\boldsymbol{B}_\mathrm{u}^{1/2} = \boldsymbol{B}_\mathrm{u}$). To this point the definition is general. However, for practical considerations, it is necessary to simplify the structure of the balance matrix K and the background error covariance matrix $\boldsymbol{B}_{\mathrm{u}}$.

The background error covariance matrix $\boldsymbol{B}_{\mathrm{u}}$ is assumed to be block diagonal with no correlation between the parameters. Thus, the background error covariance matrix is given by

$$\boldsymbol{B}_{\mathrm{u}}=\begin{bmatrix} C(\zeta) & 0 & 0 & 0 \\ 0 & C(\eta_{\mathrm{u}}) & 0 & 0 \\ 0 & 0 & C(T,p_{\mathrm{s}})_{\mathrm{u}} & 0 \\ 0 & 0 & 0 & C(q) \end{bmatrix}. \tag{7}$$

The balance relationship K is defined so that the balanced part of the divergence η and the temperature and surface pressure (T, p_{s}) is given by the equations:

$$\eta_{\mathrm{b}}=M\zeta,$$

$$(T,p_{\mathrm{s}})=N\zeta+P\eta_{\mathrm{u}}, \tag{8}$$

where the subscript u represents the unbalanced part of the variable and the subscript b the balanced part. N, P, and M are matrices to be defined later.

The K matrix which transforms

$[\zeta, \eta_{\mathrm{u}}, (T, p_{\mathrm{s}})_{\mathrm{u}}, q]$

into

$[\zeta, \eta, (T, p_{\mathrm{s}}), q]$

then becomes:

$$K=\begin{bmatrix} \boldsymbol{I} & 0 & 0 & 0 \\ M & \boldsymbol{I} & 0 & 0 \\ N & P & \boldsymbol{I} & 0 \\ 0 & 0 & 0 & \boldsymbol{I} \end{bmatrix}, \tag{10}$$

where $C(\ )$ represents the background autocovariance matrix for each variable. While the background error covariances for the unbalanced parts of the variable are independent, the balance equation (8)–(9) results in a strong multivariate coupling between the full mass and wind variables. Note that currently the q analysis is independent of the other variables (except for some coupling due to the observation term: in the radiative transfer when using radiance data, and in the hydrostatic equation when using surface pressure data). The matrix multiplication of $\boldsymbol{B}_{\mathrm{u}}$ by K allows one to write explicitly the implied background error covariance matrix $\boldsymbol{B}$ in terms of the model variables $[\zeta, \eta, (T, p_{\mathrm{s}}), q]$:

$$\boldsymbol{B}=K\boldsymbol{B}_{\mathrm{u}}K^{1}=\begin{bmatrix} C(\zeta) & C(\zeta)M^{\mathrm{T}} & C(\zeta)N^{\mathrm{T}} & 0 \\ MC(\zeta) & MC(\zeta)M^{\mathrm{T}}+C(\eta_{\mathrm{u}}) & MC(\zeta)N^{\mathrm{T}}+C(\eta_{\mathrm{u}})P^{\mathrm{T}} & 0 \\ NC(\zeta) & NC(\zeta)M^{\mathrm{T}}+PC(\eta_{\mathrm{u}}) & NC(\zeta)N^{\mathrm{T}}+PC(\eta_{\mathrm{u}})P^{\mathrm{T}}+C[(T,p_{\mathrm{s}})_{\mathrm{u}}] & 0 \\ 0 & 0 & 0 & C(q) \end{bmatrix} \tag{11}$$

The additional elements included in $\boldsymbol{B}$ over those in $\boldsymbol{B}_{\mathrm{u}}$ are the "balanced" parts of the covariances. For instance, the vorticity covariances $C(\zeta)$ and the unbalanced temperature covariances $C(T, p_{\mathrm{s}})_{\mathrm{u}}$ are both homogeneous and isotropic, whereas the $NC(\zeta)N^{\mathrm{T}}$ "vorticity-balanced" (T, p_{s}) matrix term depends on latitude. This variation with latitude results from the definition of the N matrix (see below) and the calibration of the N matrix versus forecasts differences containing a latitudinal variation because of the Coriolis force. The $NC(\zeta)N^{\mathrm{T}}$ contribution is predominant in the extratropics and negligible near the equator. This term along with the less important coupling between the divergence and temperature $PC(\eta_{\mathrm{u}})P^{\mathrm{T}}$ is responsible for the mass/wind coupling in the analysis procedure.

Each autocovariance matrix in the $\boldsymbol{B}_{\mathrm{u}}$ matrix is defined in a similar manner. Generally the C matrices are defined again as a series of matrix multiplications given by

$$C=S^{-\mathrm{T}}V^{\mathrm{T}/2}S^{\mathrm{T}}EDE^{\mathrm{T}}S^{-1}V^{1/2}S, \tag{12}$$

where S represents the spectral to grid transformation, V is a diagonal matrix of variances of the unbalanced variable on the model gaussian grid, and E is the matrix of eigenvectors and D is a diagonal matrix of eigenvalues of the vertical covariance matrices in spectral space of the unbalanced variables normalized by the variances in grid space. The E and D matrices are assumed to vary with the total wavenumber n. Thus, there is no correlation between different spectral coefficients but a full vertical autocovariance matrix is defined for each spectral coefficient. The resulting autocovariance model is nonseparable, homogeneous and isotropic in gridpoint space when the gridpoint variances do not vary in the horizontal. Thus, when the variances are horizontally constant, the correlation structures depend on scale, but not on the geographical location. The shape of the horizontal correlations is determined by the covariance spectra. The same block diagonal representation was used in the previous J_b formulation at ECMWF (Rabier and McNally, 1993; Courtier et al, 1998) but for different variables. The covariance coefficients are computed statistically using the NMC method (Parrish and Derber, 1992; Rabier et al, 1998) on 24/48-h forecast differences to estimate the total covariances for each total wavenumber n, and assuming an equipartition of errors between the $(2n+1)$ associated spectral coefficients for each zonal wavenumber m. It should be emphasized that the NMC method does not produce the true covariances but has been found to produce a useful approximation to the true covariances. However, the NMC method should produce an excellent approximation to the true dynamical balances between the variables since the model represents these balances well.

The M, N and P operators used to define the balance have a restricted algebraic structure. M and N are both the product of a so-called horizontal balance operator $\mathscr{H}$ by vertical balance operators $(\mathscr{M}, \mathscr{N})$:

$$M = \mathscr{M}\mathscr{H}, \tag{13}$$

$$N = \mathscr{N}\mathscr{H}. \tag{14}$$

The $\mathscr{H}$ operator is a block-diagonal matrix of identical horizontal operators transforming the spectral coefficients of vorticity, independently at each level, into an intermediate variable P_b which is a linearized mass variable defined below. The horizontal operators in $\mathscr{H}$ have exactly the same algebraic structure as the standard analytical linear balance equation on the sphere, and produce the latitudinal variations of the J_b structures in spectral space,

$$\begin{aligned} P_b(n, m) = {} & \beta_1(n, m)\zeta(n, m+1) \\ & + \beta_2(n, m)\zeta(n, m-1). \end{aligned} \tag{15}$$

The $\mathscr{M}$, $\mathscr{N}$ and P operators all have the same structure: block-diagonal, with one full vertical matrix per spectral component. The vertical matrices depend only on the total wavenumber n.

The $\mathscr{M}$, $\mathscr{N}$ and P matrices and $\beta 1$ and β_2 variables are estimated from the NMC method using the same set of 24/48 h-range forecast differences. Thus, the balance given by K is calibrated against forecasts produced by the ECMWF forecast model with full physics and dynamics. The actual calibration of the J_b operator requires the following 5 steps.

Step 1: $\mathscr{H}$ operator. The horizontal balance coefficients (β_1, β_2) of $\mathscr{H}$ are computed by a linear regression between the errors in vorticity and in linearized total mass P_t, assuming the functional relationship defined by the above equation with $P_t = P_b$. Note that β_1 and β_2 are independent of level. P_t is calculated from T and p_s using the linearized hydrostatic relationship at level l,

$$P_t(l) = \sum_{i=NLEV}^{l} RT_i \Delta \log p_i + RT_{\text{ref}} \log p_s,$$

where T_{ref} is set equal to 270 K, NLEV is the number of model levels, and p_i is the set of pressures at the interfaces of the model layers. The result of the linear regression has little sensitivity to the choice of reference temperature.

Step 2: $\mathscr{M}$ operator. The vertical blocks of $\mathscr{M}$ (one for each total wavenumber n) of this operator are computed by a linear regression between the spectral vertical profiles of coefficients of P_b and divergence η. Note that the statistical sampling is better for small scales than for large scales because there are $(2n+1)$ spectral profiles to be used per total wavenumber in each forecast error pattern.

Step 3: $\mathscr{N}$ and P operators. The vertical blocks are computed for each total wavenumber n exactly like $\mathscr{M}$, except that now the linear regression is between vertical spectral profiles of P_b and $\eta_u = \eta - M\zeta$ to the profiles of temperature and surface pressure:

$$[(T, p_s)]_n^m = \mathscr{N}_n[P_b]_n^m + \mathscr{P}_n[\eta_u]_n^m. \tag{17}$$

Note that the $\mathscr{N}_n$ and $\mathscr{P}_n$ matrices are not square (the output dimension is one larger than the input) but the resulting (T, p_s) covariances are still positive definite.

Step 4: Error covariances. The vertical autocovariances of the differences for the unbalanced variables,, $[\zeta, \eta_u, (T, p_s)_u, q]$, are computed for each total wavenumber n.

Step 5: Error variances. The variances implied by the NMC method in step 4 are rescaled*. The covariances are then used as such for η_u and $(T, p_s)_u$. A slightly more complicated procedure is applied for ζ and q: the covariances are normalized to create correlations, and the variances are specified in gridpoint space in order to allow for geographical variations. The assumed background error variances for q are specified as an empirical function of the background temperature and specific humidity at each grid point. The calibration of the function has been done offline using statistics of differences between radiosonde measurements and background fields in the ECMWF assimilation system (Undén, personal communication). The assumed background error variances for vorticity ζ are produced by a so-called *cycling* algorithm that relies on a Hessian-based method to estimate analysis error variances (Fisher and Courtier, 1995), and on a simple error growth model to provide short-range forecast error variances for the next analysis. A short description of the cycling algorithm is provided in Section 7.

In addition to these 5 steps, some additional minor modifications are performed on the covariances. The vertical correlations of humidity are set to zero above 100 hPa, and the standard deviations of humidity background errors are set to a very low value in the stratosphere in order to avoid spurious stratospheric humidity increments because of the tropospheric observations. The variance spectra are slighty modified to ensure that the horizontal error correlations of ζ, η_u and (T, p_s) are compactly supported (set to zero beyond 6000 km). This operation removes residual sampling noise in the error covariances. No other processing is performed except for a spectral truncation if the analysis resolution is lower than the statistics resolution (currently T106).

It is necessary to use more independent error estimates than the number of levels in the J_b calibration procedure, particularly at very large scales. The first J_b tests were carried out using 45-day samples (24/48-h forecast differences taken one day apart from each other) during December 95/January 96, March/April 96, June/July 96, September/October 96 and December 96/January 97. An extensive subjective comparison of the statistics between these 5 periods showed that there was no significant impact of the seasonal cycle (except in the grid error variances) because the J_b design does not distinguish between the northern and southern hemispheres. However, there was some difference between the December 95/January 96 period and the other ones because of the change in the ECMWF analysis system from OI to 3D-Var (at the end of January 1996). Consequently, it has been decided to neglect the seasonal effects (except in the grid point variances) and to recompute the statistics using one single 180-day homogeneous sample, leaving out the December 95/January 96 data. The 180-day statistics were implemented in May 97 and are used in all following diagnostics.

Changing the sample size from 45 to 180 days resulted in only minor modifications to the statistics. There was a reduction of the noise in the diagnostic plots that are not averages, e.g., in the spectral dependence of the vertical correlations. More importantly, there are some significant changes in the vertical correlation matrices for wavenumbers n between 0 and 3. For higher wavenumbers, the changes are not noticeable. Correspondingly, the differences between the analysis increments are mainly found in the large scales. These differences may be important for the assimilation of tidal waves, although the impact has not been fully investigated.

* The rescaling is a multiplication by an empirical factor of 0.81. The performance of the assimilation system is sensitive to the choice of this parameter. The value used in this work has been chosen in order to reproduce the scaling in the previous ECMWF assimilation system. A better scaling procedure would need to rely on a methodology along the lines of Rutherford (1972), in order to reflect the error variances of the 6-h forecasts used to produce the background fields at ECMWF.

3. Diagnosis of the formulation of J_b

Each of the various components of the definition of J_b has been analyzed to determine the component's characteristics. In this section, some of the results of this analysis will be presented.

3.1. Balance operators

3.1.1. Horizontal balance $\mathscr{H}$. This operator is defined by the spectral distribution of coefficients β_1 and β_2 in the relationship

$$P_b(n,m)=\beta_1(n,m)\zeta(n,m+1)$$
$$+\beta_2(n,m)\zeta(n,m-1), \quad (18)$$

where the coefficients outside the truncation domain are set to zero. The above equation has the same structure as the one implied by the linear balance equation on a sphere, i.e., the balance between the Coriolis force and the pressure gradient on pressure surfaces. In the new formulation of J_b, the balance is applied on model levels, which are close to pressure levels except near the ground and over steep orography.

For the linear balance equation analytical coefficients b_1 and b_2, which are the equivalents of β_1 and β_2, can be shown to be:

$$b_1(n,m)=\frac{b}{n(n+1)}\left(1-\frac{1}{n+1}\right)$$
$$\times\sqrt{\frac{(n+1+m)(n+1-m)}{(2n+3)(2n+1)}}, \quad (19)$$

$$b_2(n,m)=\frac{b}{n(n+1)}\left(1+\frac{1}{n}\right)$$
$$\times\sqrt{\frac{(n+m)(n-m)}{(2n+1)(2n-1)}}, \quad (20)$$

where $b=-2\Omega R_a^2$, Ω is the rotation speed of the Earth, R_a is its radius.

Fig. 1 shows the spectral distribution in (n,m) space of the quantities $|\log_{10}(\beta_1/b_1)|$ and $|\log_{10}(\beta_2/b_2)$. There is a significant sampling noise, particularly in the smaller scales. Except along the edge of the spectrum, the differences between the statistically calculated values and the analytical values are small. The larger values at the edges (up to 50% difference) are probably an artifact of the linear regression being carried out in terms of one predictor instead of two in the rest of the spectral triangle.

Another characterization of the horizontal balance can is provided by the comparison of maps of balanced geopotential height when either $\mathscr{H}$ or the analytical balance operator are applied to the same vorticity field. This was done for one particular field of analyzed vorticity increments, and the subjective impression was that the balanced height maps (not shown) are very similar. The patterns are almost identical everywhere. The largest height differences were found around 240 hPa, with an absolute maximum of 1.33 m, which is small compared to the actual height increments. The height increments produced with $\mathscr{H}$ tend to be slightly smaller than with the analytical balance. This is probably because the linear regression is performed over all levels including levels near the surface which have weaker geostrophic coupling.

At this time, it appears that the analytical values

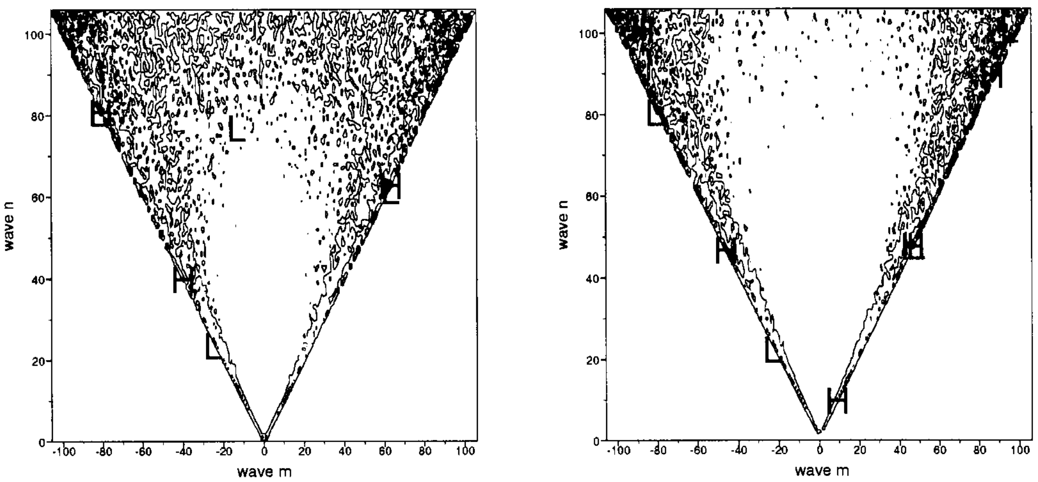

Fig. 1. Relative distance between the factors (β_1,β_2) and their respective analytical counterparts (b_1,b_2): the left panel shows $|\log_{10}(\beta_1/b_1)|$, the right panel shows $|\log_{10}(\beta_2/b_2)|$. The contour interval is 0.2, the lowest isoline is at 0.1, i.e., it delineates 10% differences.

could have been used in the system with little change in the results.

Daley (1997) argued that it is inappropriate to use the analytical balance or the Hough modes to enforce geostrophism in variational analysis increments in the tropical regions. First, he pointed out that the exact algebraic inverse of the analytical balance cannot be used to calculate nondivergent wind differences from geopotential differences because the balance operator is ill-conditioned near the equator (Fig. 4 of Daley, 1997). Then he designed a modified linear balance operator with its pseudo-inverse in order to alleviate the problem. With the formulation described here, a singular value analysis of the statistical horizontal balance operator $\mathscr{H}$ would show that the J_b formulation suffers from the same problem as with the analytical balance. The cross-covariances between vorticity and mass (i.e., (T, p_s)) are of the form $C(\zeta)N^T$ which is directly comparable with the term $\boldsymbol{F}_{u\Phi}$ in eq. (5.6) of Daley (1997). An analysis carried out with a single wind observation on the equator yields mass increments which are comparable with the left-hand column of Fig. 7 in Daley (1997), containing what is described by Daley as a "fallacious equatorial wind-height coupling". However, the amplitude of the height increment is extremely small (less than 3% of the increment at 50N with a similar wind departure) and can be neglected for all practical purposes. If a moderate change in the height field near the equator were projected on the balanced modes, a large change in the winds would result. This change in the wind would cause a large increase in the value of J_b. Therefore, the height changes near the equator are primarily projected into the unbalanced modes which produces little change in the winds and a relatively small increase in J_b.

3.1.2. The complete balance operator. The statistical balance operator can be measured objectively by diagnosing the amount of explained variance in the actual meteorological fields. The explained variance shows to what extent the assumed balance relationship really exists in nature (actually in the ECMWF model) and gives an indication of the optimality of the assumed algebraic form of the relationship. The r.m.s. distance between the balanced fields and the real ones is provided by the variance v_u of the residual, the unbalanced fields. We compare it to the total variance v_t by the following quantity called the explained variance ratio:

$$1 - \frac{v_u}{v_t}. \tag{21}$$

In order to measure accurately the performance of the balance, the calculation of the explained variance and the calibration of the balance operators are performed using independent datasets. The actual relative size of the balanced and unbalanced terms in J_b is not just a property of the balance operator, it depends on the algebraic restrictions made on the covariance operators (their spatial homogeneity in particular).

The spectral and vertical distribution of these quantities is presented in Fig. 2 with the global mean explained variance being 9.3% for divergence, 59% for temperature and 90% for surface pressure. The divergence is weakly explained by vorticity at all scales, mainly near the ground at synoptic scales and near the tropopause at small scales. The (T, p_s) variables are better explained at synoptic than small scales. In the vertical, the synoptic-scale temperature is well explained at all levels except near the ground because of surface processes like friction. The small-scale temperature is well explained in the stratosphere. The explanation for this phenomenon is unknown but may be related to the stronger diffusion in the forecast model at these levels and scales.

The latitudinal performance of the balance operator is shown in Fig. 3. Because of poor sampling, the graphs are noisy near the poles, and therefore the figures only extend from 80N to 80S. The explained divergence ratio has a maximum in the mid-latitudes near the jet stream and near the surface with little explained variance at other locations. For the temperature, the explained variance is again primarily in the extratropics with the variance best explained in the troposphere away from the surface.

3.2. *Structure of covariances*

The covariance matrices are defined for each of the analysis variables (vorticity, unbalanced divergence, unbalanced temperature and surface presssure, and specific humidity) for each total wavenumber. In this section, the structure of these covariance matrices will be examined. For the

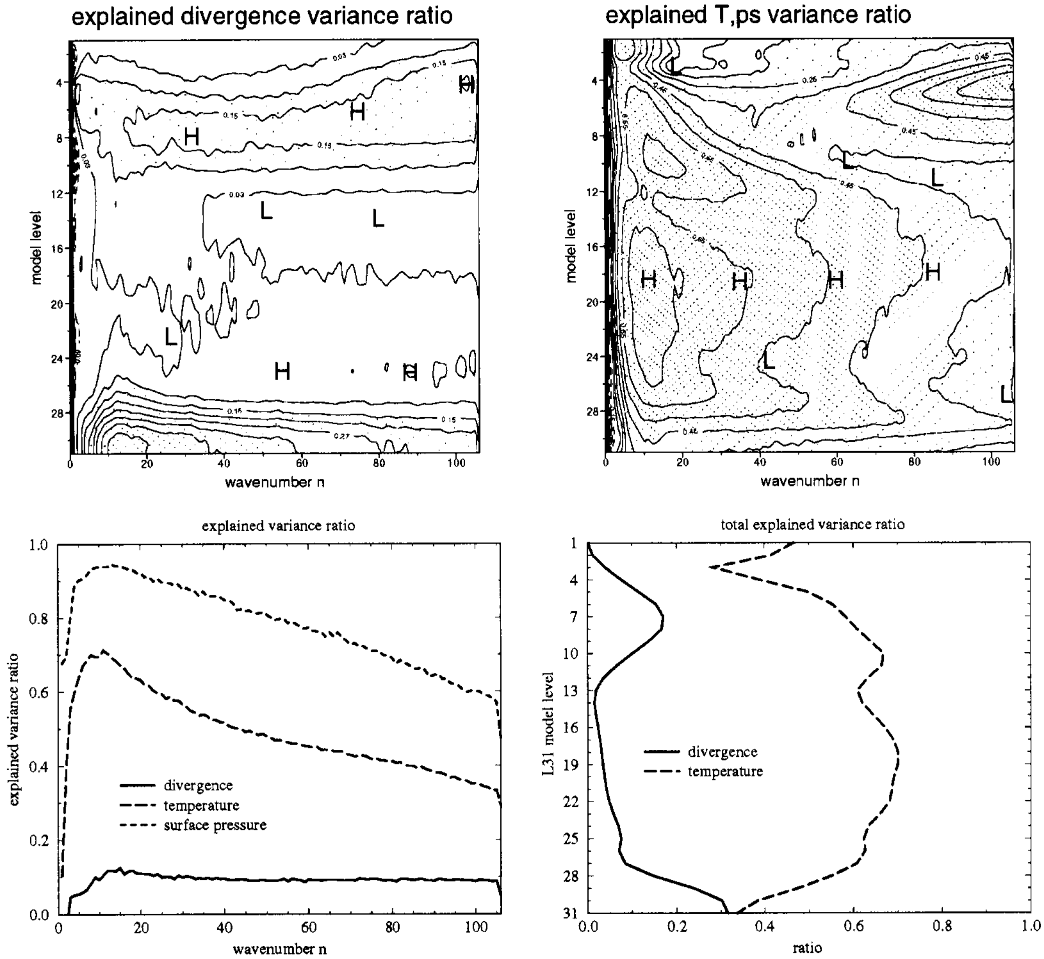

Fig. 2. Distribution of the explained variance ratios (as defined in the text) for divergence (top left) temperature (top right), stratified according to total wavenumber (bottom left, including p_s) and to model level (bottom right).

unbalanced temperature and surface pressure, the covariances will be compared to the full temperature and surface pressure covariances. For the divergence fields, the unbalanced covariance matrices are similar in structure to the full covariance matrices and for this reason will not be discussed. Note that the covariances discussed in this section are for a T106 truncation, while in operations at ECMWF the analysis is performed at T63. Thus, in operations, only the covariance matrices up to T63 are used resulting in slightly smoother analyses.

The vertical distribution of total standard deviations is plotted in Fig. 4 for the vorticity, divergence, unbalanced divergence, temperature, unbalanced temperature and specific humidity. For surface pressure, the total and unbalanced values are 2 hPa and 0.62 hPa, respectively. All the variables have small variations in the vertical except ζ, which has a maximum in the upper troposphere (more or less at the mid-latitude jet levels), and q which varies over several orders of magnitude between the stratosphere and the lower troposphere. The large variation in the size of q along with its boundedness and the non-homogeneity of its statistics as a function of background humidity make it a very ill-suited variable for a linear analysis scheme such as 3D-Var. A different

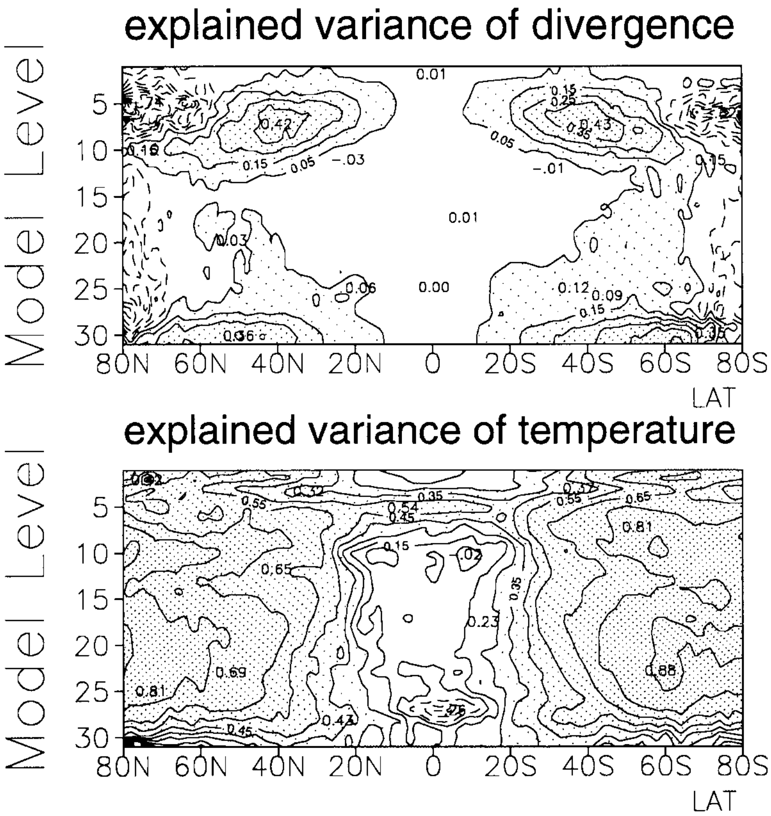

Fig. 3. Zonal average of the explained variance ratios of η (top) and temperature (bottom). The explained variance ratio for p_s is 0.2 at the equator, 0.9 in the extratropical parts of both hemispheres.

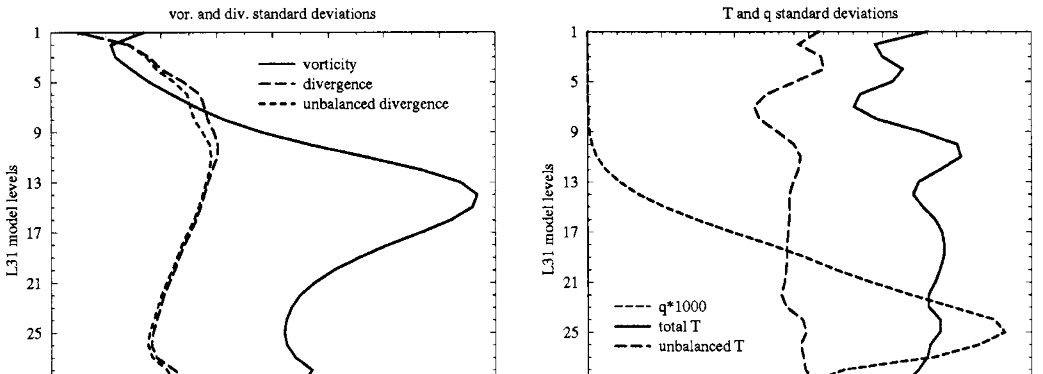

Fig. 4. Vertical background standard deviation distribution in the unscaled covariances. Left panel: vorticity, divergence and unbalanced divergence multiplied by 10^5. Right panel: q multiplied by 1000, total temperature in the extratropics and unbalanced (i.e., tropical) temperature. J_b uses these values scaled by 0.9.

choice of analysis variable may reduce these problems.

For each variable we have a set of vertical covariance matrices of forecast difference that are used as background error covariances multiplied by a global scaling of the variances (by 0.81) as explained earlier in this paper. The variances presented here are the unscaled ones. From each set of vertical covariance matrices, an average correlation matrix over all wavenumbers and a horizontal correlation structure in physical space can be diagnosed as described in Courtier et al. (1998).

The vorticity covariances are depicted in Fig. 5. The average vertical correlations of vorticity are broad except in the stratosphere. They appear even broader near the ground, however this is just a consequence of the vertical spacing of the model levels. The sharpness of the vertical correlations increases with horizontal wavenumber, except at the very large scales. This characteristic is commonly called "non-separability" and is the sign of three-dimensional isotropy in the vorticity error patterns. Most of the variance of vorticity error comes from sub-synoptic scales, between wavenumbers 20 and 60, and from the top of the troposphere (the mid-latitude jet levels). The horizontal correlations are sharp, and they are almost zero beyond 200 km in the troposphere. In the stratosphere, there is some broadening of the horizontal correlations at higher levels.

The divergence covariances (Fig. 6) are virtually identical to the covariances of unbalanced divergence, except that the total variances are slightly larger than the unbalanced ones, as already shown in Fig. 4. For this reason, only the total divergence covariances are shown. The vertical correlations are much sharper than for vorticity, and they are almost separable. The variances are distributed rather homogeneously in the vertical, except at the top, and the maximum in the variance is at smaller scales (around T60) than for vorticity resulting in horizontal correlations which have a shorter scale than for vorticity.

The humidity covariances (not shown) are sharp in the vertical and fairly broad in the horizontal, with correlations of about 0.1 at 800 km. The correlations are similar to those for vorticity, with a significant non-separability, however the variances are very different, with negligibly small values above 500 hPa. The stratospheric structures are not very meaningful because of the very small variances at these levels. The bulk of the variances is located around 800 hPa and at synoptic and subsynoptic scales, roughly between wavenumbers 15 and 80. This suggests (along with the relatively large variances at smaller scales in the divergence) that the ECMWF analysis would benefit from use of a truncation higher than T63. The humidity covariances and structure functions are not discussed further in this paper because they have almost no interaction with the rest of the formulation, and they have not been affected by the J_b reformulation.

The total (T, p_s) covariances are displayed in Figs. 7, 8. The vertical T correlations are very broad in the troposphere and in the lower stratosphere, with negative correlations between the two regions (the boundary is around level 12, i.e., 270 hPa). There is a substantial non-separability, and the broadness is mainly caused by large horizontal scale patterns between wavenumbers 5 and 20, with a large variance at all levels. Since these are global statistics, both T and p_s have a very small average variance beyond wavenumber 60. Accordingly, the horizontal T and p_s correlations are both broad with the p_s horizontal correlation having a weakly negative lobe at a distance of 2000 km. The (T, p_s) cross-correlations are generally negative, with about -0.25 correlations in the lower troposphere (at all scales except the very large ones) and around the tropopause (at large scales only). There is almost no (T, p_s) correlation between levels 13 and 21, i.e., between 300 and 630 hPa except at large scales.

The unbalanced (T, p_s) covariances are displayed in Figs. 9, 10. The variances are smaller and the correlations are different than for the total variables. The vertical correlations are much sharper with less negative correlation. The differences are primarily for wavenumbers below 20, where most of the variance is explained by the balance operator N. The (T, p_s) cross-correlations also have substantial changes, with the disappearance of the negative correlation with stratospheric temperature. These negative correlations are well explained by the vorticity through the balance equation. The (T, p_s) correlated structures in the lower troposphere are incompatible with the balance, and they are left in the unbalanced statistics, with a negative correlation of almost -0.4. The

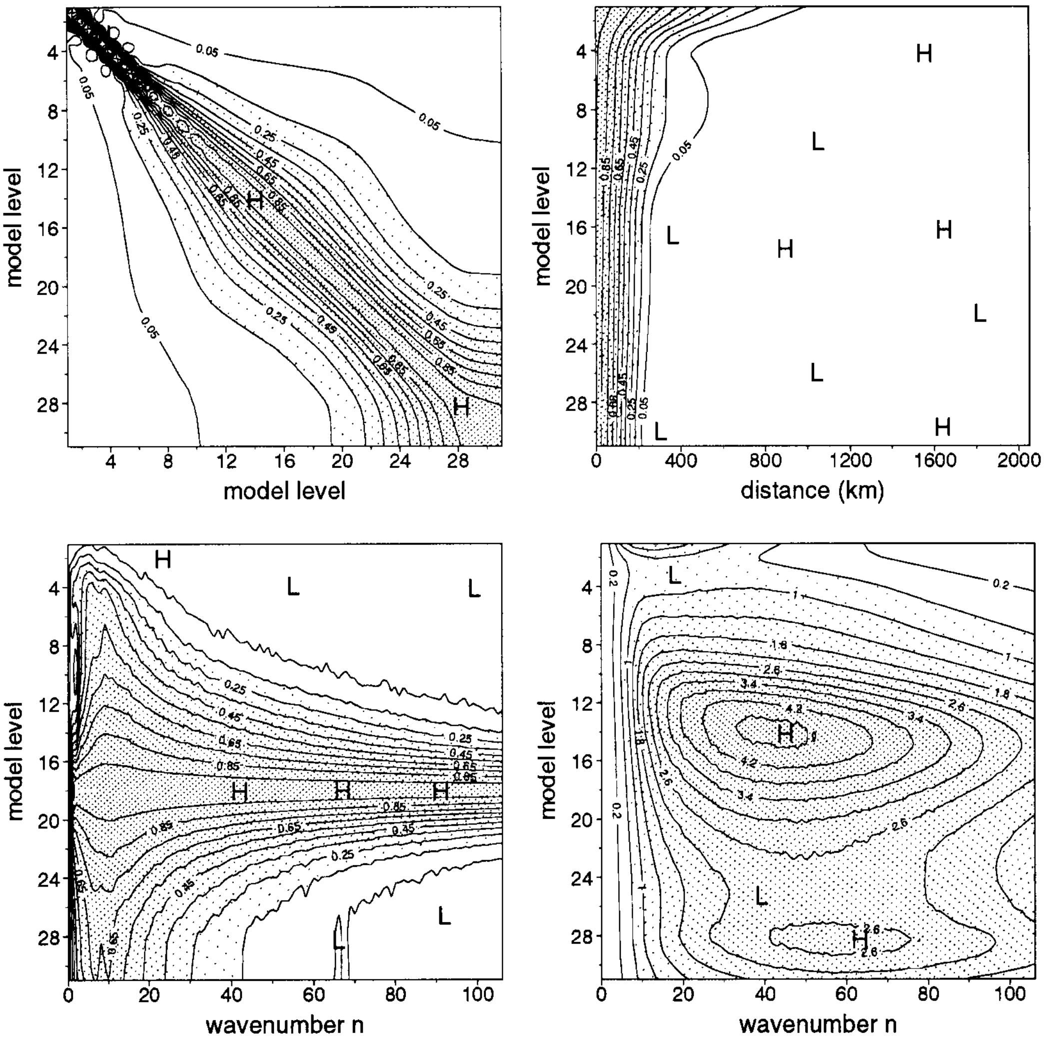

Fig. 5. Covariances of vorticity ζ: average vertical correlations (top left), radial profiles of horizontal correlations (top right), vertical correlations with model level 18 (approx. 500 hPa) (bottom left), complete distribution of the standard deviations (bottom right, $\times 10^{-6}$ S.I.). The correlation isolines values are 0.1 apart, with an isoline at 0.05, and the negative values are plotted with dashed isolines.

horizontal unbalanced correlations have a slightly smaller scale than those for the total variables.

4. Meteorological validation

4.1. Single-observation experiments

The effect of the J_b design on the actual analysis is usually difficult to interpret. The structure of the analysis increments results from a complex weighted average of the observation departures from the background when there is more than one observation in the vicinity. The effects of the J_c term and of the initialization procedure in the incremental method make the picture even more complicated.

The simplest illustration of the implied structure functions is provided by non-incremental analyses with no J_c term and one single simulated observa-

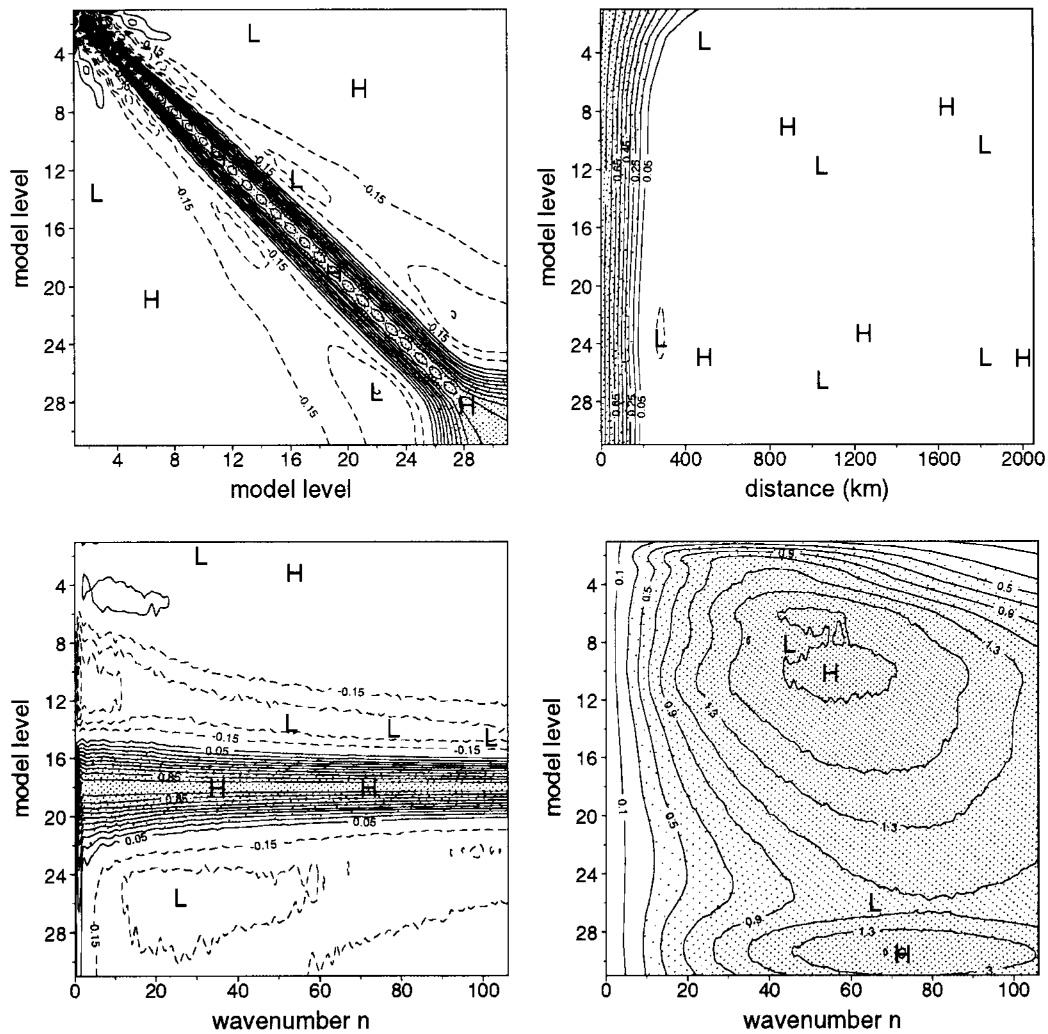

Fig. 6. Same as Fig. 5 except covariances of divergence η.

tion per analysis. In this case, the analysis increment is given by

$$x^a - x^f = \boldsymbol{B}H^T(H\boldsymbol{B}H^T + \boldsymbol{R})^{-1}(z - Hx^f). \tag{22}$$

where the usual notations have been used (x^a and x^f are the analysis and forecast state vectors, respectively, z the observation vector, H the linearized observation operator, $\boldsymbol{B}$ and $\boldsymbol{R}$ are the background and observation error covariance matrices, respectively). Since a single observation is used, $(H\boldsymbol{B}H^T + \boldsymbol{R})^{-1}(z - Hx^f)$ is a scalar and the analysis increment produces a good representation of the structure functions.

In Fig. 11, the analysis increment for a simulated 1000 hPa geopotential observation at (0N, 30W) with an observational error of 10 m and a 10 m departure from the background is shown. The effect of this observation is very similar to a surface pressure observation. The height increments are small because the assumed background errors are small for this parameter near the equator. Note that there is an implied wind from the height observation on the equator. Near and on the equator, the flow is almost entirely divergent resulting from the coupling of the divergence and temperature in the balance equation. Away from

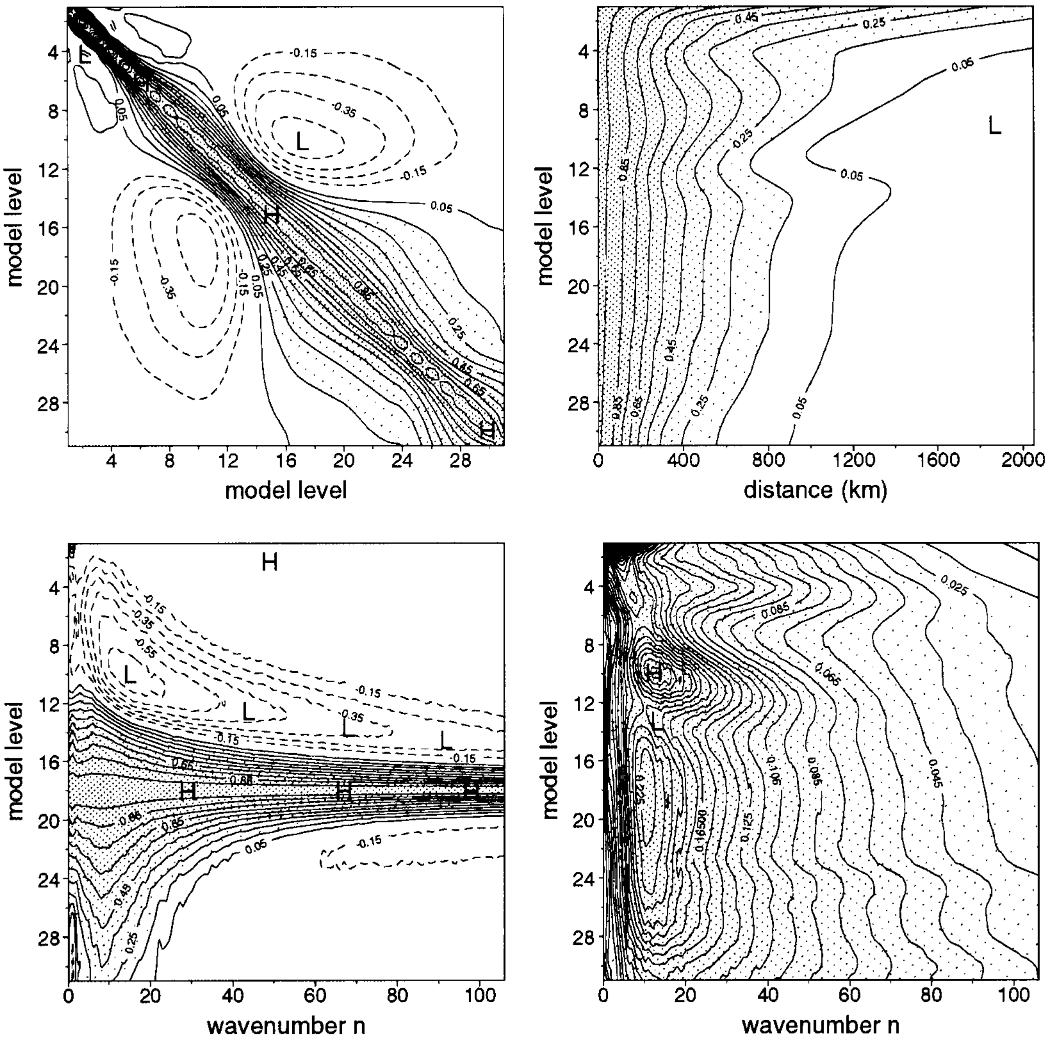

Fig. 7. Same as Fig. 5 except covariances of total temperature T (K).

the equator, the flow becomes geostrophic with the height observation creating changes in the temperature field away from the equator and the balance equation creating corresponding approximately geostrophic changes to the wind field. While the increments are small, the implied structures could be important for the analysis of tropical storms and the use of scatterometer data. Fig. 12 shows vertical cross sections of the temperature increment field from the previous and the current formulations of J_b and the divergence from the new formulation. (The old formulation would not produce a divergence increment.) The vertical T increment is as expected from the results in the previous sections. The previous and current formulations of J_b produced very different vertical structures in the temperature increments. In the divergence field, a divergent flow is now produced near the surface with compensating convergence over a deep layer higher in the troposphere.

When the $z1000$ observation is moved to latitude 60N, the increments change substantially. In Fig. 13, the temperature, vorticity and divergence increments are shown for the new formulation of

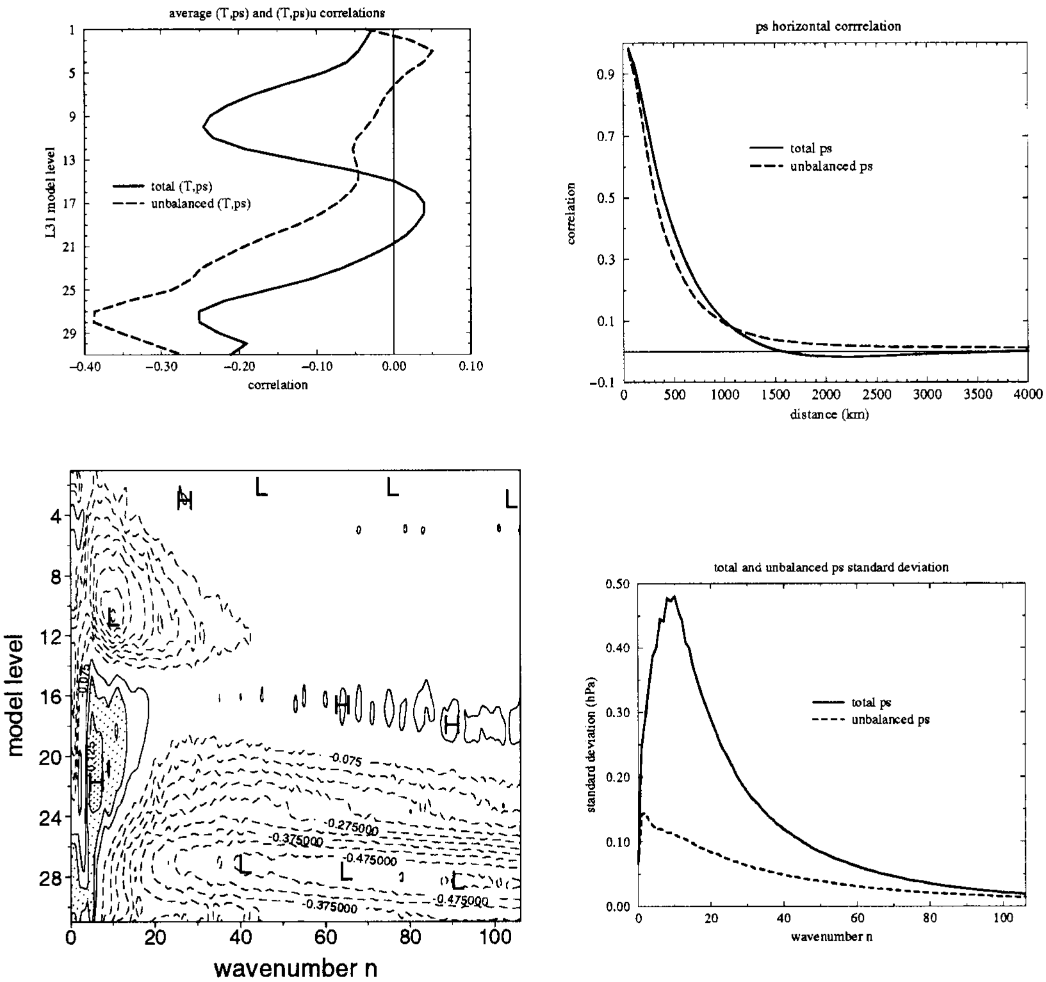

Fig. 8. Cross-covariances between temperature and surface pressure: average vertical cross-correlations (top left), radial profile of horizontal p_s autocorrelation (top right), complete distribution of the total (T, p_s) correlations (bottom left, the isolines values are 0.1 apart), and p_s standard deviation spectrum (bottom right, in hPa). The counterparts for the unbalanced (T, p_s) are also displayed in each panel, except lower left.

J_b. The previous formulation of J_b produced similar increments for the temperature and vorticity but produced no increment in the divergence field. Note that the temperature increment is similar to the temperature increment produced by the previous formulation in the tropics. The previous formulation produced an increment on the equator that was more representative of the mid-latitudes since it was globally homogeneous. The divergence field produced by the change in the height field has its maximum near the surface, has a weak compensation over a deep layer higher in the atmosphere and produces convergence (divergence) when the change in the height field produces a low (high). The divergent flow near the surface becomes weakly convergent at higher levels.

Fig. 14 shows the increments produced by a 200 hPa temperature observation with 1 K departure and observation error. This observation would be similar to an aircraft temperature report. Since the cross-correlation between the temperatures and divergence is strongest near the surface,

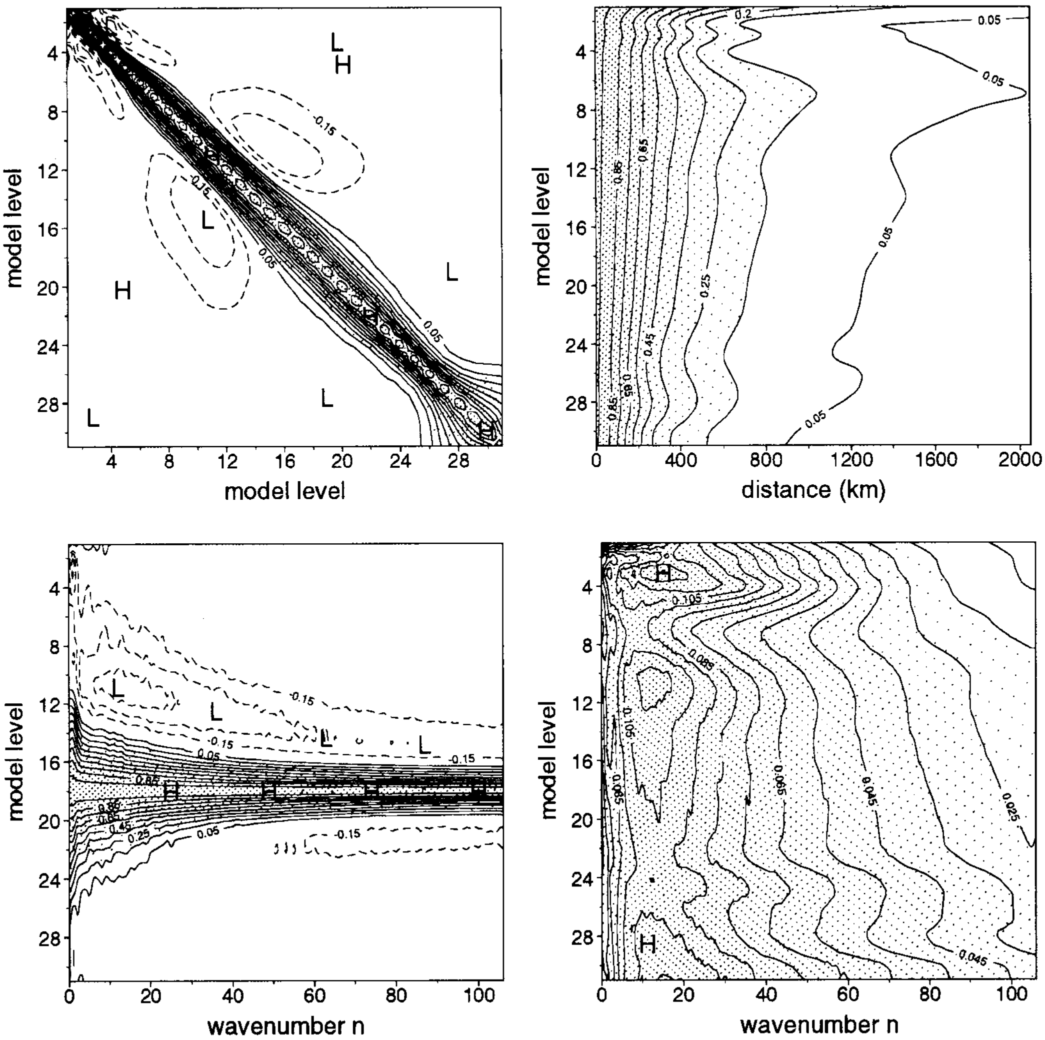

Fig. 9. Autocovariances of unbalanced temperature T, plotted as in Fig. 7.

there is only a small divergence increment. Thus, the horizontal wind increments shown in Fig. 15 appear nondivergent.

The increments generated by a single u wind component observation in the mid-latitudes and tropics are shown in Figs. 16, 17. The pattern of the wind increments are similar. The amplitude is smaller on the equator because the background standard deviations are smaller there. The equatorial wind increment is not exactly symmetric because the background standard deviations are not uniform. Notice how the extratropical mass increment is rotated in Fig. 16 in order to account for some ageostrophism (i.e., gradient wind) in the wind increment near the ground. This rotation causes some skewness in the wind increment although at the observation point it still points eastward. The mass increment at the equator is negligible.

4.2. *Impact on the assimilation*

An extensive comparison of the previous and new formulations of J_b in the ECMWF data

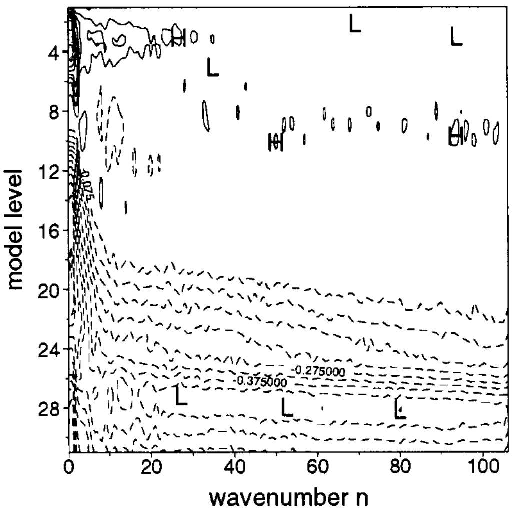

Fig. 10. Distribution of the unbalanced (T, p_s) cross-correlations. The average vertical correlation, the horizontal correlation and spectrum are displayed in Fig. 8.

assimilation system has been made. A total of 9 weeks of assimilation were run during four seasons, plus 4 weeks of preoperational assimilation before the operational implementation of the J_b revision.

An illustration of the net effect of the change in J_b formulation is given in Figs. 18, 19. They show a comparison of the analysis increments produced with exactly the same system (with the same background field and observations in particular) except for the change in J_b. Fig. 18 shows the wind and temperature increments at two pressure levels. The increments are quite similar in most areas of the mid-latitudes except the wind in the mid-western USA. In the tropical regions, the increments are reasonably similar near the ground, but they are very different at high levels. The wind structures are smoother and more marked with a much more convincing subtropical jet structure in the new formulation. Fig. 19 shows that the largest wind differences at 150 hPa are usually located in the sub-tropical regions. In this region, the old analysis system artificially transitioned between a multivariate to a univariate analysis. In the average, the largest wind differences are located between 40N and 40S and between 100 and 500 hPa.

The average amplitude of the increments is generally similar between the two systems except in the tropical regions where the increments are substantially smaller with the new J_b. In the tropics, the new formulation produces somewhat smoother analyses given the same observation departures. Also, in the assimilation, the forecast fits the data substantially better (Fig. 20) in the tropics resulting in smaller observation departures from the background. Both of these effects result in smaller increments in the tropics.

The cost of the revised J_b is less than the previous one. However, the impact on the overall cost of the 3D- or 4D-Var assimilation is small because it is dominated by the handling of the observations (for 3D-Var) and by the direct and adjoint model runs (in 4D-Var). The improved preconditioning speeds up the experimental analyses with a small number of observations, but the convergence of the full 3D-Var is not clearly faster than with the previous J_b.

The fits to the background of both TOVS radiances and tropical humidity observations are a bit improved, although it may be just a side-effect of the overall improvement in the assimilation of wind and temperature. In the assimilations based on the old and new J_b formulations the zonally averaged temperature, humidity and Hadley cell circulations are very similar, with no significant difference found. In the forecasts, the short-range spin-up of the precipitation is slightly reduced. The new J_b formulation behaves better than the previous one with respect to the assimilation of TOVS radiances. With the use of the new formulation and a revision of the radiance bias correction scheme in summer 1997, the ECMWF operational assimilation was able to assimilate TOVS radiances directly rather than SATEM retrievals in the stratosphere (G. Kelly and B. Harris, personal communication).

4.3. Impact on the forecasts

The J_b revision has a major positive impact on the quality of the forecast at all ranges. Fig. 21 shows the forecast scores computed over the 3D-Var experiments with the revised J_b formulation immediately prior to operational implementation. In the mid-latitudes, there was a significant improvement in the forecast skill in the medium range forecasts for both hemispheres. In the tropics, there appears to be a loss of skill at short

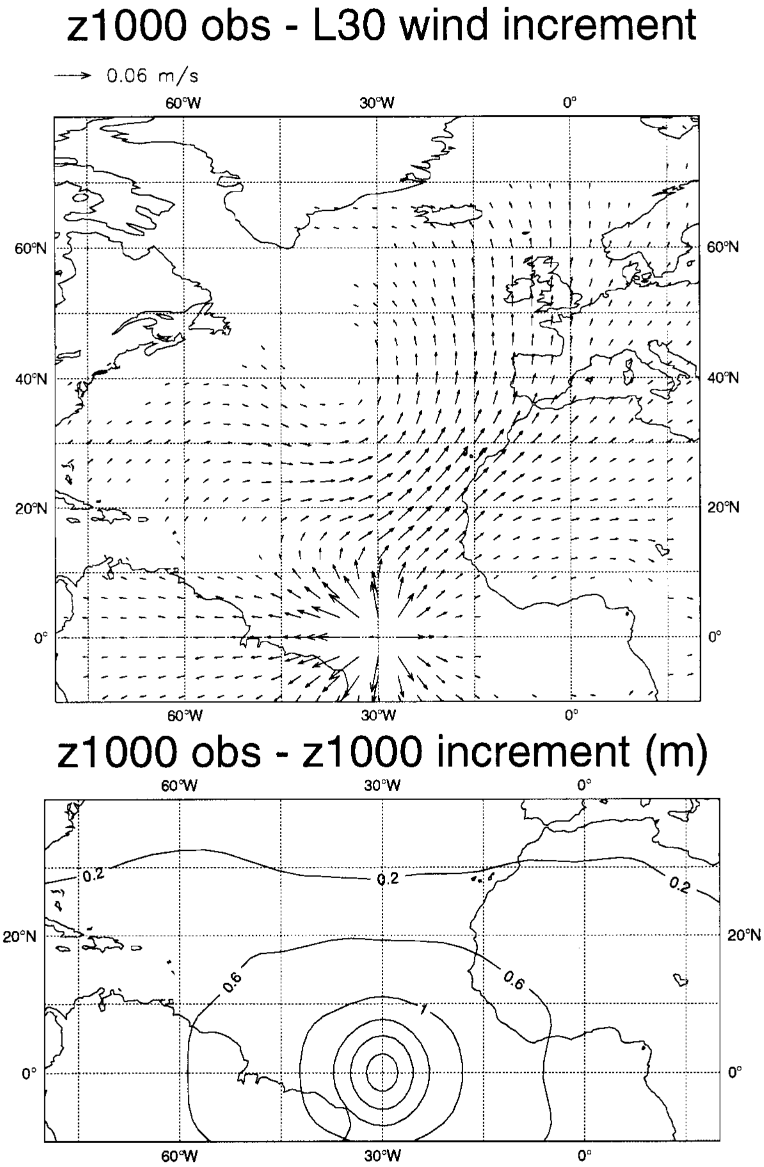

Fig. 11. Wind (top) and $z1000$ geopotential height increment generated by a $z1000$ geopotential observation simulated at (0N, 30W) that is 10 m higher than the background. The increment is almost symmetric with respect to the equator.

ranges, however this is a result of the verification procedure. The verifying analysis in all cases was the operational analysis. In the tropics, the analyses were substantially changed, which explains the apparent loss of skill in the short range. However as shown previously in comparisons with tropical observations, the forecasts were actually improved in the tropics. If the verifying analysis is taken from the system with the revised J_b, the scores of the new system (not shown) are improved in the short range (up to day 3) and virtually unchanged in longer ranges.

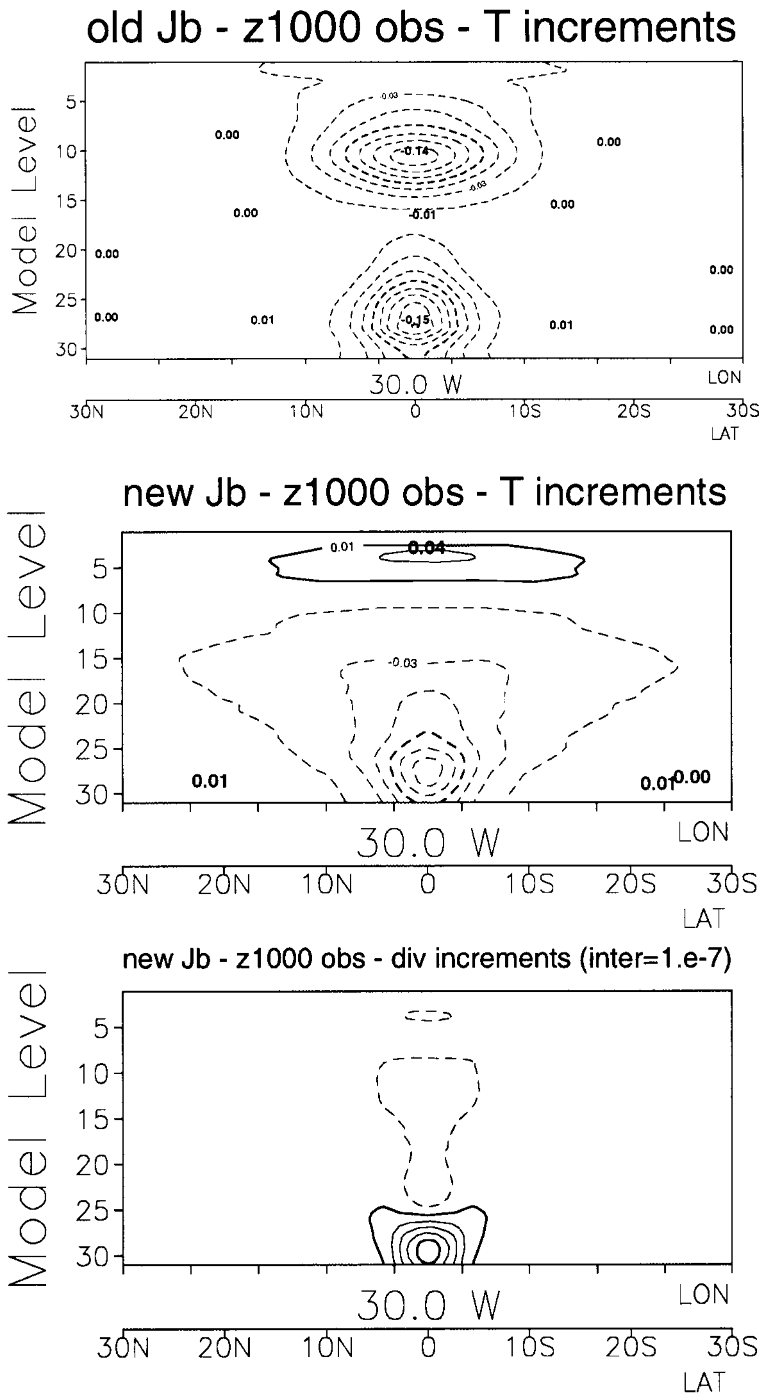

Fig. 12. Vertical north–south cross-sections of increments of temperature and divergence with the previous ("old") and current ("new") J_b, generated by a $z1000$ observation simulated at (0N, 30W) that is 10 m higher than the background.

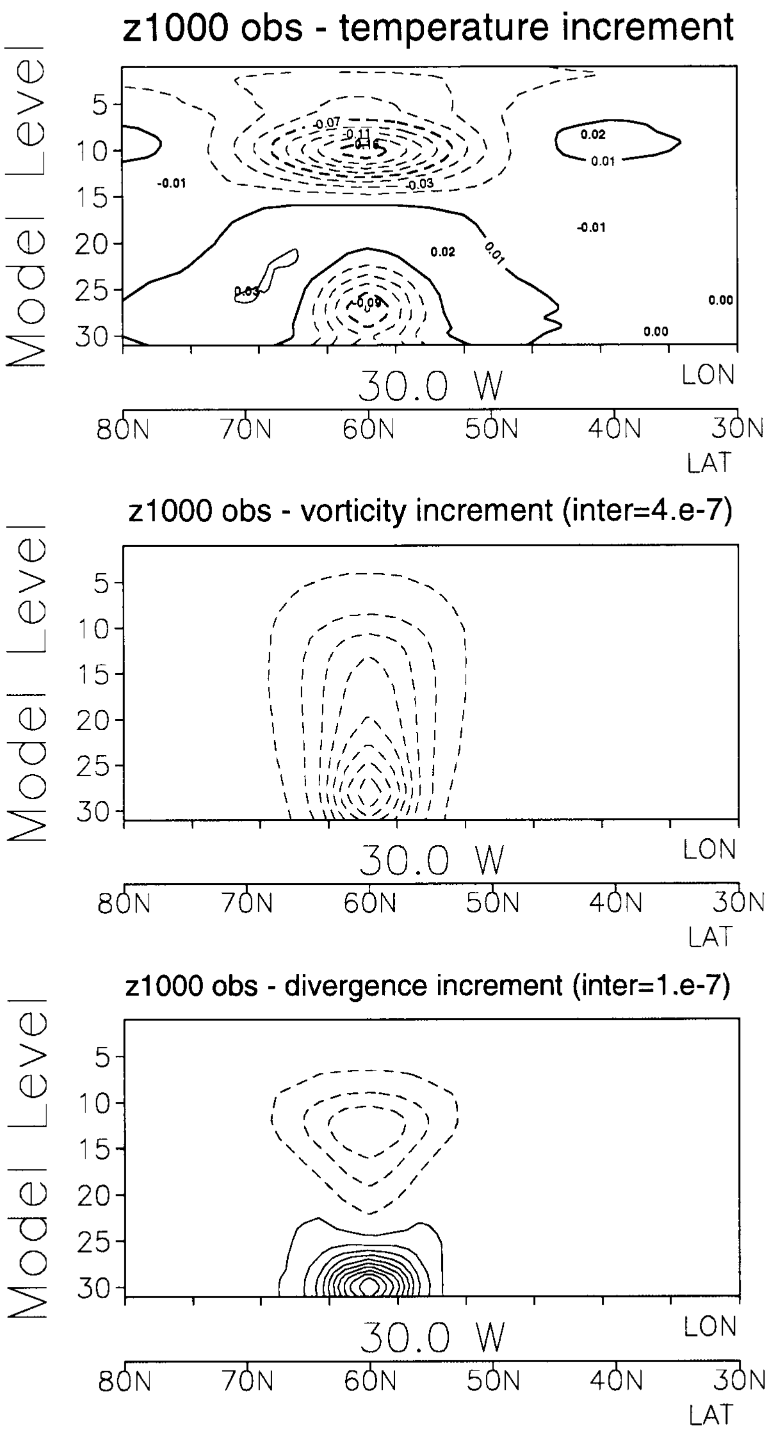

Fig. 13. Temperature, vorticity and divergence increments generated by a $z1000$ observation simulated at (60N, 30W) that is 10 m higher than the background.

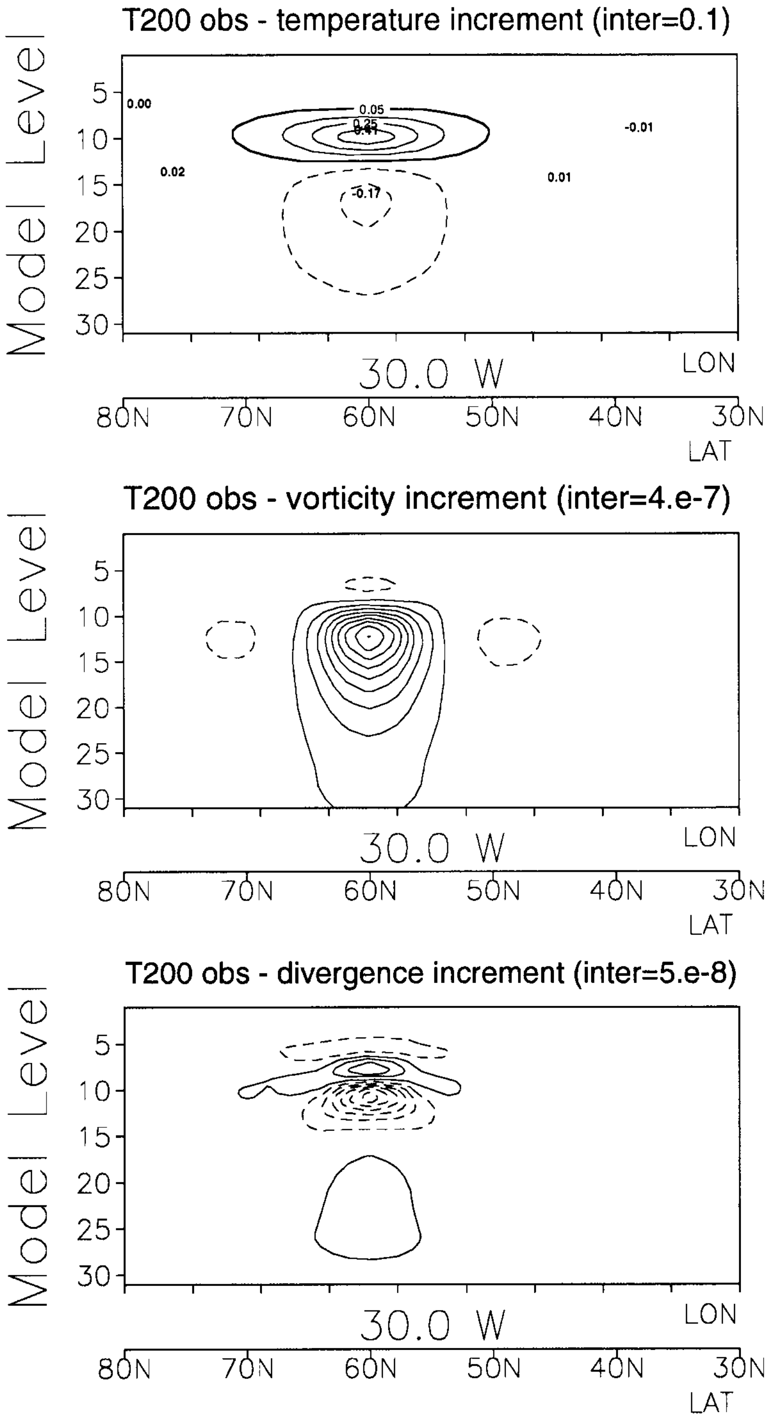

Fig. 14. Temperature, vorticity and divergence increments generated by a simulated 200 hPa temperature observation at (60N, 30W) that is 1 K warmer than the background.

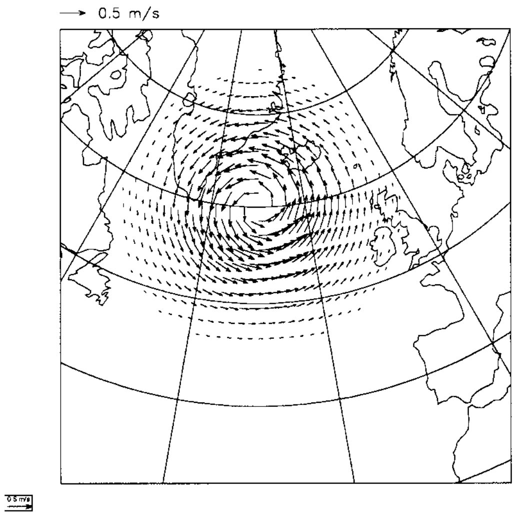

Fig. 15. Wind increment at level 13 (approx. 300 hPa) generated by a simulated 200 hPa temperature observation at (60N, 30W) that is 1 K warmer than the background.

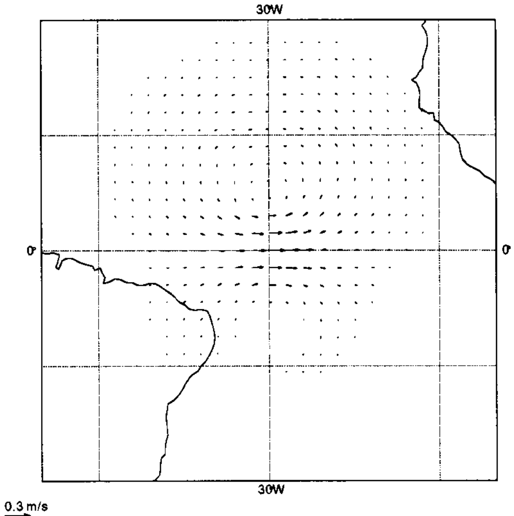

Fig. 17. Wind increment at model level 30 generated by a simulated u component wind observation at 10 m above ground, at (0N, 30W) that is 1 ms^{-1} stronger to the east than the background wind. The surface pressure increment is not plotted because the maximum amplitude ress than 0.01 hPa).

5. Conclusions and discussion

A reformulation of the background error covariance for the ECMWF data assimilation system has been described. In this formulation, the analysis variables are redefined so that a balanced part of the temperature, surface pressure and divergence are implied from the vorticity field. By doing this an implied latitudinally dependent structure in the temperature and surface pressure is directly included in the analysis procedure while still defining homogeneous and isotropic covariance functions. Also some coupling between the divergence and the vorticity fields is included especially near the surface and near the tropopause.

The reformulation of J_b brings a notable improvement to the quality of the assimilation

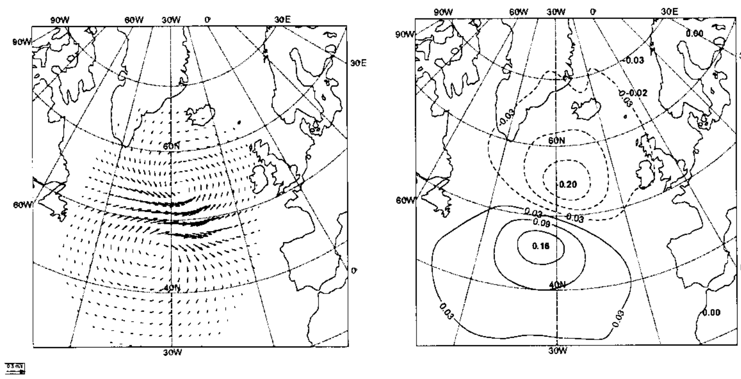

Fig. 16. Increments generated by a simulated u component wind observation at 10 m above ground, at (50N, 30W) that is 1 ms^{-1} stronger to the east than the background wind. Left: wind increment at model level 30 (largest vector is 0.3 ms^{-1}), right: surface pressure increment (in hPa).

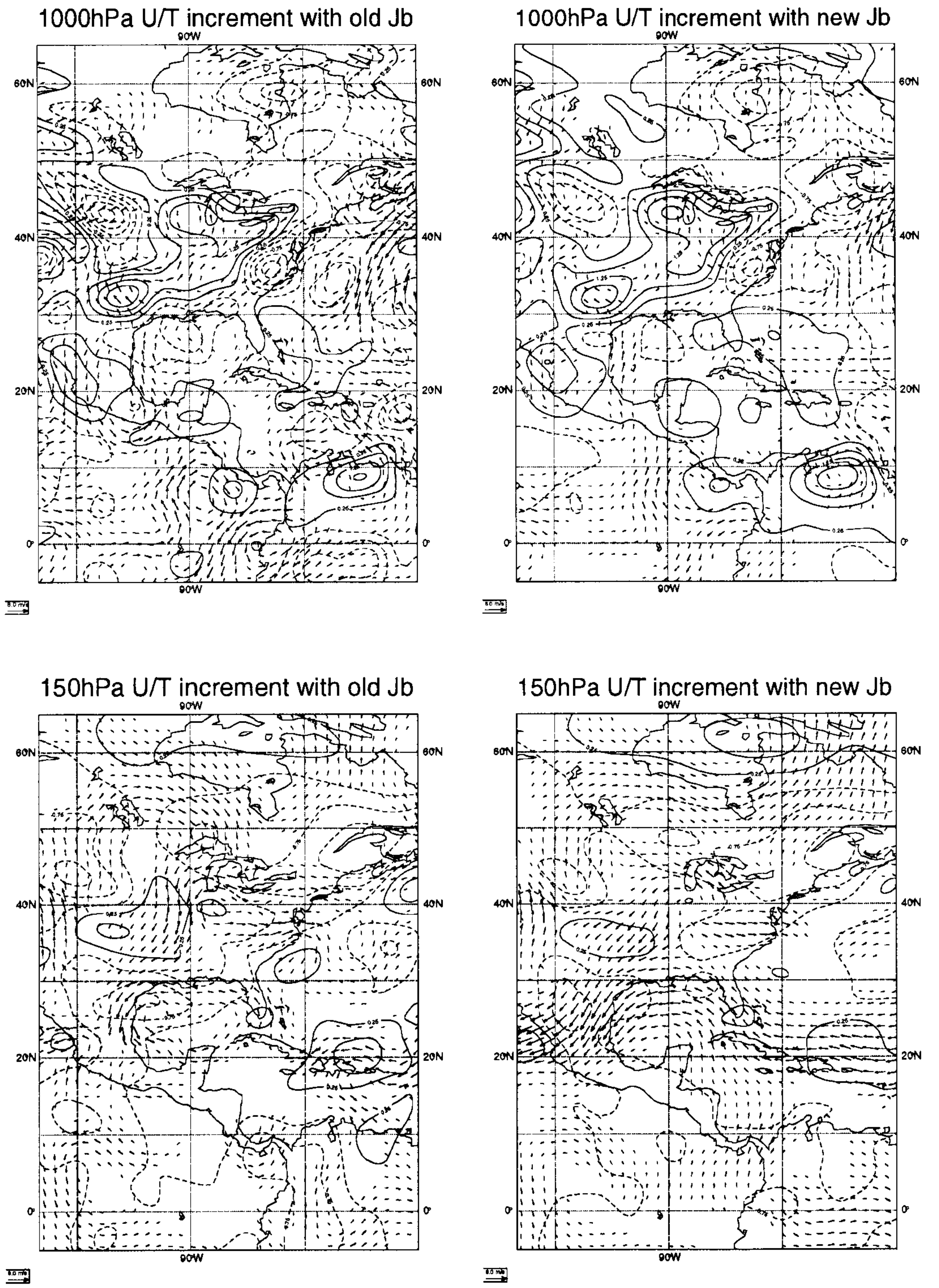
1000hPa U/T increment with old Jb
1000hPa U/T increment with new Jb
150hPa U/T increment with old Jb
150hPa U/T increment with new Jb
90W
60N
40N
20N
0°

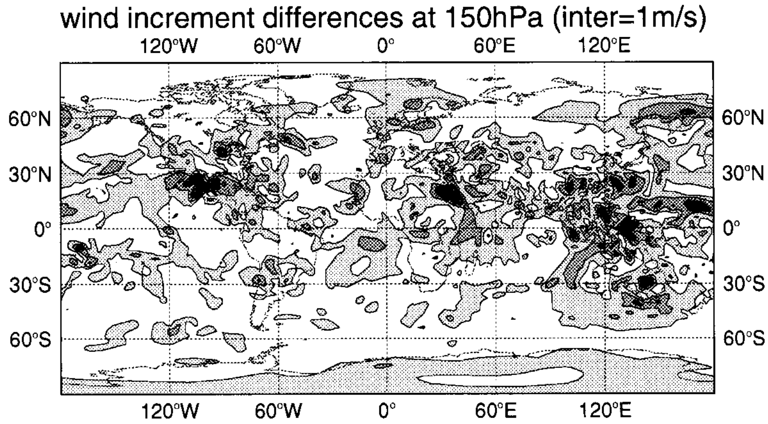

Fig. 19. Distribution of the differences between the 150 hPa wind analyses on 1 February 1997 00UTC with the old and new J_b formulation. The darker the shading, the larger the difference.

and of the ensuing forecasts. However, some weaknesses remain. The structure functions are too uniform despite the tropical/extratropical contrast which is implied by the formulation. It would be desirable to include a situation dependent background error covariance with different length scales at different location.

There is room for much improvement of the analysis of humidity in the current assimilation system. In the reformulation described here, the analysis of humidity has not been modified. A better choice for the humidity variable should be used, and a balance constraint between the humidity variable and the other variables would be useful. However, the balance of the moisture to the other analysis variables is probably different between the tropics and extratropics making the formulation and implementation of such a balance much more difficult (especially in spectral space).

The basic characteristics of J_b strongly depend on assumptions made about the NMC method. The NMC method clearly has limitations and should be only considered as a temporary solution for defining the background error statistics. Considerable future work is necessary to improve the definition of the background error covariances. However, the NMC method probably gives a reasonable estimate of the balances between the analysis variables at least to the extent that the balance is included in the forecast model.

The improvements in J_b benefit 4D-Var and the Kalman filter directly. Technically the knowledge of the exact square root of the background error covariance matrix facilitates the work on numerical preconditioning and simplifications to the Kalman filter. However, there are some doubts as to how appropriate the J_b formulation is for the generation of useful flow-dependent structure functions, because it is too barotropic. In dynamically unstable areas, we need to make the J_b covariances more isotropic in phase space (i.e., with sharper correlations in physical space).

6. Acknowledgements

A key ingredient of the J_b implementation at ECMWF was the cycling algorithm implemented and tuned by M. Fisher following early suggestions by P. Courtier. Some of the ideas in this work are based on ideas incorporated in the NCEP analysis system by D. Parrish. Thanks are due to the NCEP and ECMWF management for allowing J. Derber to spend a year developing the

Fig. 18. Comparison of the 3D-Var analysis increments on 1 February 1997 00UTC between the old (left panels) and new J_b formulation (right panels), at levels 150 hPa (top) and 1000 hPa (bottom), for wind and temperature. The contour interval is 0.5 K.

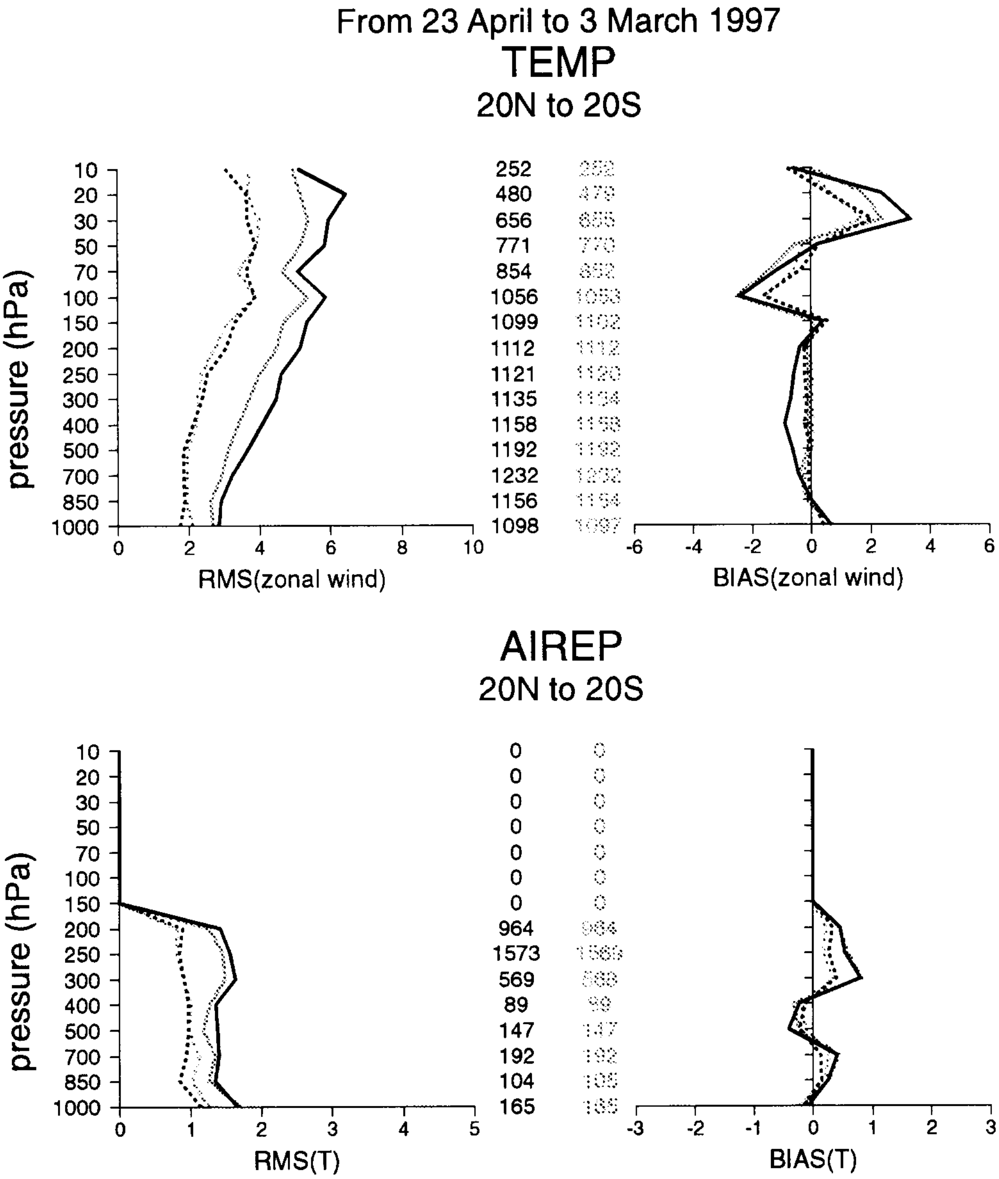

Fig. 20. Impact of the J_b revision on the observation fits to the analysis (dotted curves) and background (solid curves) for the tropical TEMP winds (top) and the tropical AIREP temperatures (bottom). The black curves are for the previous operations, the gray curves are for the parallel suite. The statistics have been computed over a 10-day period. The number of observations used at each level are plotted in the center of each panel.

J_b formulation at ECMWF. The real-size implementation and experimentation was made possible thanks to the help and technical support from the whole IFS/Arpège team, notably L. Isaksen, M. Hamrud, E. Andersson, F. Rabier, P. Undén, A. Simmons, H. Järvinen and J. Haseler. A large portion of the existing J_b code developed by W. Heckley was incorporated in the new ver-

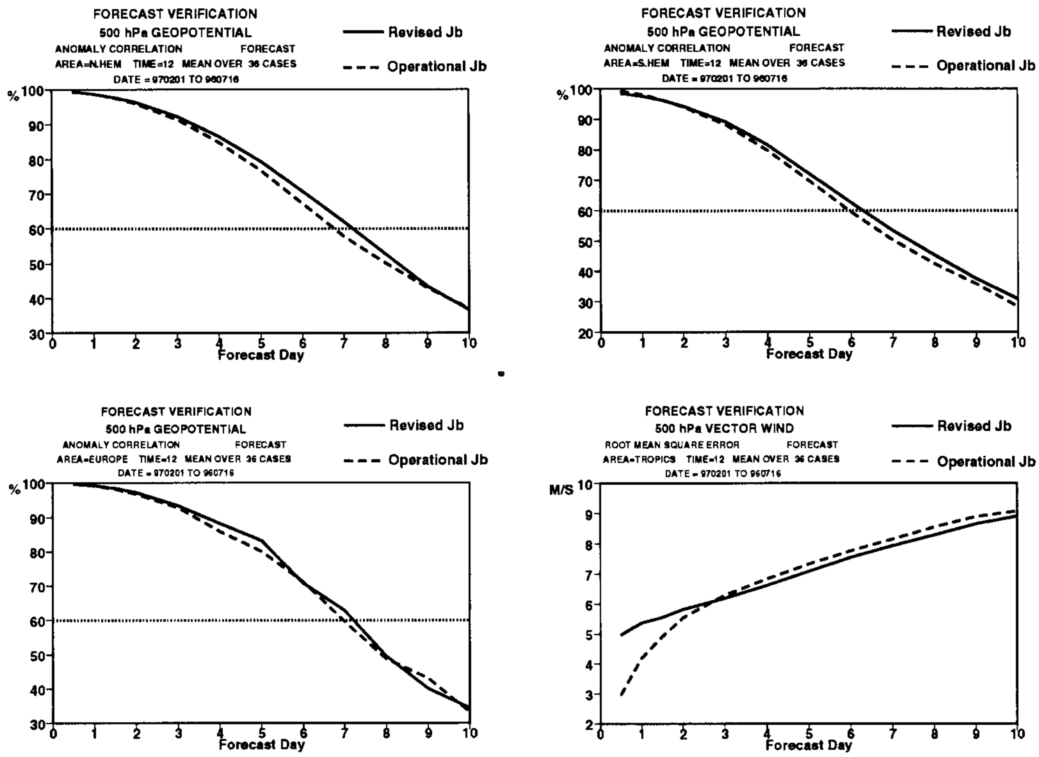

Fig. 21. Impact on the forecast scores on the J_b revision over 5 weeks of experimental assimilation (2 weeks in February 1997, 3 weeks in June/July 1996).

sion of the analysis. The manuscript benefitted from suggestions by D. Parrish, R. Treadon, A. Simmons and the anonymous reviewers.

7. Appendix

The cycling algorithm

The cycling algorithm (Fisher and Courtier, 1995) uses the past history of the observing network and the climatological variances of the fields in order to estimate the spatial distribution of the short-range forecast errors in the assimilation system. As explained below, the cycling procedure is intimately coupled with the specification of the J_b cost-function. The specification of the background error variances for vorticity ζ is carried out in gridpoint space. However, for consistency with the multivariate formulation, the vertical profile of r.m.s. averaged standard error at each level is kept equal to the scaled values estimated from the NMC method. The horizontal pattern of background standard errors is provided externally from a so-called cycling algorithm that estimates the distribution of analysis and background errors using the following method:

(1) For each analysis, we compute an approximation of the Hessian of the cost-function in the space of the χ variable as follows:

$$J''_\chi \approx 2\left[\boldsymbol{I} + \sum_{i=1}^{k} (\lambda_i - 1) v_i v_i^{\mathrm{T}}\right] \tag{23}$$

(if there is no J_o term, then $J'' = 2\boldsymbol{I}$), where the v_i are the eigenvectors associated with the k largest eigenvalues of the Hessian. The eigenvalues and eigenvectors are computed approximately using a conjugate-gradient minimization of a low-resolution (T42L31) version of the variational problem with linearized observation operators. In this case, the cost-function is strictly quadratic: finite differences of the gradient ∇J are equal to evaluations of the Hessian operator, so that the conjugate-gradient minimization is equivalent to a Lanczós method for the determination of the largest eigenvalues of the Hessian matrix (Fisher and Courtier, 1995). The number k of eigenvectors is limited by the number of iterations allowed. Typically, 70 iterations are performed and 22 eigenvectors are computed with an acceptable accuracy.

(2) The approximation of the Hessian is converted to physical space using $x = L\chi$, so that

$$J'' \approx 2\left[\boldsymbol{B}^{-1} + \sum_{i=1}^{k} (\lambda_i - 1)(Lv_i)(Lu_i)^{\mathrm{T}}\right], \tag{24}$$

which is invertible using the Shermann–Morrison–Woodbury formula. The inverse is of the form

$$2(J'')^{-1} \approx \boldsymbol{B} - VV^{\mathrm{T}}, \tag{25}$$

where the matrix V contains k columns which are linear combinations of the vectors (Lv_i).

(3) The columns of V are transformed to gridpoint space, squared and subtracted from the field of background error variances yielding an approximation of the analysis error variances. As expected the difference between the background and analysis error variances is positive and concentrated over data-rich areas. Negative "analysis error variances" are set to a small positive values.

(4) The 6-h forecast error variances are estimated by inflating the analysis error variances using the error growth model of Savijarvi (1995) for the evolution of standard errors:

$$\frac{\mathrm{d}\sigma}{\mathrm{d}t} = (a + b\sigma)\left(1 - \frac{\sigma}{\sigma_\infty}\right). \tag{26}$$

The asymptotic values σ_∞ are set to $\sqrt{2}$ times the climatological standard deviation of the field itself (with artificially increased values in the tropics). We use $a = 0.1$ times the global mean background error per day, and $b = 0.4$ per day.

(5) The forecast standard error maps estimated for vorticity are normalized by their global average at each level and multiplied by the scaled values implied by the NMC method.

It is worth noting that the forecast error variances for all parameters are also used in the preliminary quality control of the observations: the rejection thresholds for large first-guess departures are expressed in multiples of the background standard errors, in order to accept outlier data more easily in data-sparse areas (Järvinen and Undén, 1997).

REFERENCES

Andersson, E., Haseler, J., Undén, P., Courtier, P., Kelly, G., Vasiljević, D., Branković, C., Cardinali, C., Gaffard, C., Hollingsworth, A., Jakob, C, Janssen, P., Klinker, E., Lanzinger, A., Miller, M., Rabier, F., Simmons, A., Strauss, B., Thépaut, J.-N. and Viterbo, P. 1998. The ECMWF implementation of three dimensional variational assimilation (3D-Var). Part III: Experimental results. *Q. J. R. Meteor. Soc.*, in press.

Bouttier, F., Derber, J. and Fisher, M. 1997. *The 1997 revision of the J_b term in 3D/4D-Var.* ECMWF Research Dept. Technical Memorandum no. 238, 1–54. Available from ECMWF, Shinfield Park, Reading RG2 9AX, UK.

Courtier, P., Andersson, E., Heckley, W., Pailleux, J., Vasiljevic, D., Hollingsworth, A., Fisher, M. and Rabier, F. 1998. The ECMWF implementation of three-dimensional variational assimilation (3D-Var). Part I: formulation. *Q. J. R. Meteor. Soc.*, in press.

Daley, R. 1997. Generation of global multivariate error covariances by singular-value decomposition of the linear balance equation. *Mon. Wea. Rev.* **124**, 2574–2587.

Fisher, M. and Courtier, P. 1995. *Estimating the covariance matrix of analysis and forecast error in variational data assimilation.* ECMWF Research Dept. Technical Memorandum no. 220, 1–26. Available from ECMWF, Shinfield Park, Reading RG2 9AX, UK.

Heckley, W., Courtier, P., Pailleux, J. and Andersson, E. 1992. The ECMWF variational analysis: general formulation and use of background information. *Proceedings of the ECMWF workshop on variational data assimilation*, 9–12 November 1992, pp. 49–93. Available from ECMWF, Shinfield Park, Reading RG2 9AX, UK.

Järvinen, H. and Undén, P. 1997. *Observation screening and background quality control in the ECMWF 3D-Var data assimilation system.* ECMWF Research Dept. Technical Memorandum no. 236, 1–33. Available from ECMWF, Shinfield Park, Reading RG2 9AX, UK.

Parrish, D. and Derber, J. 1992. The National Meteorological Center's spectral statistical interpolation analysis system. *Mon. Wea. Rev.* **120**, 1747–1763.

Rabier, F. and McNally, T. 1993. *Evaluation of forecast error covariance matrix.* ECMWF Research Dept. Technical Memorandum no. 195, 1–30. Available from ECMWF, Shinfield Park, Reading RG2 9AX, UK.

Rabier, F., McNally, A., Andersson, E., Courtier, P., Undén, P., Eyre, J., Hollingsworth, A. and Bouttier, F.

1998. The ECMWF implementation of three-dimensional variational assimilation (3D-Var). Part II: structure functions. *Q. J. R. Meteor. Soc.*, in press.

Rutherford, I. 1972. Data assimilation by statistical interpolation of forecast error fields. *J. Atmos. Sci.* **29**, 809–815.

Savijärvi, H. 1995. Error growth in a large numerical forecast system. *Mon. Wea. Rev.* **123**, 212–221.